Pergamon

Int. J. Solids Structures Vol. 34, No. 25, pp. 3215–3233, 1997

0020–7683/97 $17.00 + .00

PII: S0020–7683(96)00208–9

RELAXATION OF THERMAL STRESSES IN DISSIMILAR MATERIALS (APPROACH BASED ON STRESS INTENSITY)

TADANOBU INOUE and HIDEO KOGUCHI†
Department of Mechanical Engineering, Nagaoka University of Technology, 1603-1 Kamitomioka, Nagaoka, Niigata, 940-21, Japan

(*Received* 28 *December* 1995; *in revised form* 27 *August* 1996)

Abstract—The characteristics of thermal stresses near apex in dissimilar materials composed of arbitrary wedge angles under thermal loading are investigated theoretically and numerically. The thermal stresses σ_h ($h = rr, r\theta, \theta\theta$) near the apex are represented by $K_{hj}r^{p_j-1}$, where p_j-1 is the order of stress singularity and K_{hj} indicates the intensity of stress field with $j = 1, 2, \ldots, n$. For the metal/ceramics composite, combinations of the bonded wedge angle, in which K_{hj} becomes zero, are clarified theoretically, and the disappearance conditions of stress singularity from both the order p_j and the intensity K_{hj} are examined. Also, classification of the distribution of the intensity K_{hj} which divided into two forms is shown for p_1 and p_2, respectively, on the $\varphi_1+\varphi_2$–φ_1 plane. © 1997 Elsevier Science Ltd.

1. INTRODUCTION

In dissimilar materials, the stress singularity frequently occurs under surface tractions and thermal loading due to discontinuity of materials on the interface. The stress fields σ_h ($h = rr, r\theta, \theta\theta$) near the apex, in dissimilar materials, are defined by a linear combination of the singular solutions $K_{hj}r^{p_j-1}$ of type r^{p-1} corresponding to roots p_j in $0 < \mathrm{Re}(p) < 1$ and $K_{hg}\log r$ of type $\log r$ to a double root at $p = 1$, no singularity ones $K_{hj}r^{p_j-1}$ to roots p_j in $\mathrm{Re}(p) > 1$ and particular ones K_{hpa} to a root at $p = 1$ and K'_{hg} to a double root at $p = 1$ (Bogy, 1970; Inoue *et al.* 1994; 1995), where p_j is the j-th root of an eigen equation and K_h for each solution indicates the intensity of the stress field. Bogy (1971a), and Hein and Erdogan (1971) derived the eigen equation for a two-phase bonded structure with arbitrary wedge angles, and they have clarified the relationship between the order of stress singularity and the combinations of materials with wedge angles and mechanical properties. Bogy (1971b), Fenner (1976), and Cook and Erdogan (1972) investigated two bonded half planes containing a semi-infinite crack terminating at an interface, and showed that the order of stress singularity at the tip of the crack existing in the stiff side of the two-phase materials becomes large in comparison with that in the soft side. Blanchard and Ghoniem (1989) examined thermal stress singularities in finite bonded quarter planes by using an eigenfunction expansion method.

As mentioned above, studies on the order of stress singularity have so far been carried out by the above investigators and others (Inoue and Koguchi, 1996; Koguchi *et al.*, 1996; Pageau *et al.*, 1994a; 1994b; Williams, 1952), and the relationship between the order of stress singularity and the combinations of materials has been made clear. However, the characteristic on the intensity of the stress field in dissimilar materials is not made clear. In particular, a relation between the stress intensity and the combinations of materials has not yet been theoretically clarified for dissimilar materials with arbitrary wedge angles.

In this paper, the equations for thermal stresses near the apex, in semi-infinity dissimilar materials composed of two homogeneous isotropic wedges with arbitrary angles under a uniform temperature change (Fig. 1), are theoretically derived using the Airy stress function through the Mellin transform. The uniform temperature change is then assumed to act on the whole of the bonded structure. Next, for the bonded structure of Cu/Si_3N_4 composed

† Author to whom correspondence should be addressed.

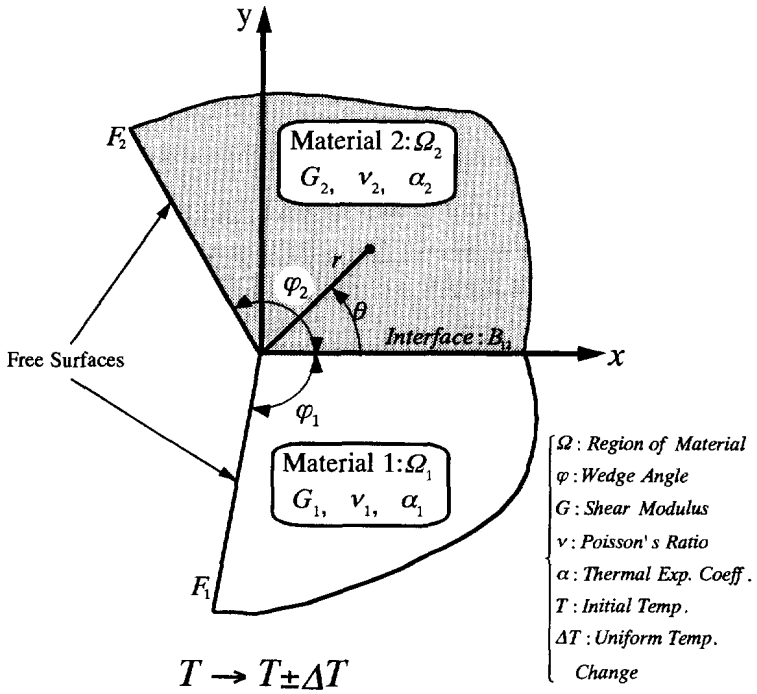

Fig. 1. Model for a two-phase bonded structure under a uniform temperature change.

of three-quarters planes, a relation between the order of stress singularity and the wedge angle φ_1 of material 1 is investigated, and the distributions of the stress intensities K_{h1} and K_{h2} for roots p_1 and p_2 are examined as to how they vary with the wedge angle φ_1. It is shown that the distribution of the intensity K_{hj} is classified by two forms for those of root p_1 and p_2, respectively. Also, the singular solutions can disappear even if the root p_j of the eigen equation exists in the range $0 < \mathrm{Re}(p) < 1$, by finding the combinations of the bonded wedge angles yielding $K_{hj} = 0$. Hence, it is very important for improving the reliability of dissimilar materials to investigate the bonded wedge geometry yielding $K_{hj} = 0$. So, the relationship between the wedge angle φ_1 of material 1 and the total angle $\varphi_1 + \varphi_2$ of the bonded wedge, in which K_{hj} become zero, is studied in detail for the Cu/Si_3N_4 composite. After that, classification of the distribution of the intensity K_{hj} is shown on the $\varphi_1 + \varphi_2 - \varphi_1$ plane, and the disappearance conditions of stress singularity from both the order of singularity and the stress intensity are clarified.

2. THERMOELASTIC THEORY IN DISSIMILAR MATERIALS

The theoretical solutions of the thermal stresses in dissimilar materials under thermal loading are defined by the process shown in Table 1 (Inoue *et al.*, 1995), as follows

In the case of a singularity of type r^{p-1}

$$\sigma_h(r,\theta) \Big/ \frac{E_2 \alpha_2 \Delta T}{1+\nu_2} = \sum_{j=1}^{n} K_{hj} \rho^{p_j - 1} + K_{hpa}. \tag{1}$$

In the case of a singularity of type $\log r$

$$\sigma_h(r,\theta) \Big/ \frac{E_2 \alpha_2 \Delta T}{1+\nu_2} = K_{hg} \log \rho + K'_{hg}, \tag{2}$$

where h represents each stress component $(rr, r\theta, \theta\theta)$ and the dimensionless variable ρ is

Table 1. Derivation process of thermal stresses in a two-phase bonded structure under a uniform temperature change

1

Airy stress function ϕ^*, stresses $(\sigma_{rr}^*, \sigma_{r\theta}^*, \sigma_{\theta\theta}^*)$ and displacements (u_r^*, u_θ^*) through the Mellin transform

↓ For boundary condition of stresses and displacements

2

$$[\Delta]_{8\times 8}\{\omega\} = \{L\}$$

$$\{\omega\} = \{a_1, b_1, c_1, d_1, a_2, b_2, c_2, d_2\}^T$$

$$\{L\} = \{0, 0, 0, 0, T_{12}, 0, 0, 0\}^{1T}$$

$$T_{12} = \frac{E_2\alpha_2\Delta T}{1-\nu_2}\left[\frac{k_{12}\left(n_1\frac{\alpha_1}{\alpha_2} - n_2\right)}{p(p-1)}\right]a^{-(p-1)}$$

$$k_{12} = \frac{G_1}{G_2}, \quad n = \begin{cases} 1+\nu & \text{for plane strain} \\ 1 & \text{for plane stress} \end{cases}$$

↓ According to Cramer's Principle

3

$$\begin{cases} a(p)_\delta = \frac{1}{S}T_{12}M_{a\delta}, \quad b(p)_\delta = \frac{1}{S}T_{12}M_{b\delta} \\ c(p)_\delta = \frac{1}{S}T_{12}M_{c\delta}, \quad d(p)_\delta = \frac{1}{S}T_{12}M_{d\delta} \end{cases}$$

S: Eigen equation, δ $(=1, 2)$: Each region number

↓ From reversion of the Mellin transform

4

$$\sigma_{rr}(r, \theta) = \frac{-1}{2\pi i}\int_{c-i\infty}^{c+i\infty}\sigma_{rr}^*(p, \theta)r^{p-1}\,dp \quad \text{etc.}$$

$$0 < \mathrm{Re}(p), \quad 0 < r < \infty$$

given by

$$\rho = \frac{r}{a}(r \ll a), \tag{3}$$

where a is a radius of a uniform temperature change acting to the semi-infinity bonded structure and must be much more than distance r. The first term in eqn (1) is the solution corresponding to the j-th root p_j of an eigen equation in the range of $0 < \mathrm{Re}(p) < 1$ (singularity) and $\mathrm{Re}(p) > 1$ (no singularity), the second term which is independent of distance r is a particular solution corresponding to a root of $p = 1$ which is always the root of the eigen equation, and eqn (2) is a solution corresponding to a double root of $p = 1 (p \to 1)$. The K_{hj}, K_{hpa}, K_{hg} and K'_{hg} for each solution in eqns (1) and (2) are the dimensionless stress intensities which depend on the wedge angles of the materials, their mechanical properties (Young's modulus, Poisson's ratio and thermal expansion coefficient) and the angle coordinate θ. As is seen from eqns (1) and (2), the thermal stresses near the apex are calculated from the sum of each solution for root p_j of the eigen equation. The eigen equation of the two-phase bonded structure is derived by expanding and arranging the determinant of the coefficient matrix Δ of an 8×8 system of Step 2 in Table 1 (Bogy, 1971a), defined as

$$S(\varphi_1,\varphi_2,\alpha_{12},\beta_{12};p) = A(\varphi_1,\varphi_2;p)\beta_{12}^2 + 2B(\varphi_1,\varphi_2;p)\alpha_{12}\beta_{12} + C(\varphi_1,\varphi_2;p)\alpha_{12}^2 + 2D(\varphi_1,\varphi_2;p)\beta_{12} + 2E(\varphi_1,\varphi_2;p)\alpha_{12} + F(\varphi_1,\varphi_2;p), \quad (4)$$

where α_{12} and β_{12} are parameters shown by Dundurs (1969), defined as

$$\alpha_{12} = \frac{k_{12}m_2 - m_1}{k_{12}m_2 + m_1}, \quad \beta_{12} = \frac{k_{12}(m_2-2) - (m_1-2)}{k_{12}m_2 + m_1}, \quad (5)$$

with

$$m_\delta = \begin{cases} 4(1-\nu_\delta) & \text{for plane strain} \\ 4/(1+\nu_\delta) & \text{for plane stress} \end{cases}, \quad (6)$$

where k_{12} represents the stiffness ratio (see Step 2 in Table 1) and δ represents each region number ($\delta = 1, 2$). In Table 1, a function T_{12} of Step 2 which is dependent on the thermal expansion coefficient is led from the interface condition for the r-direction displacement through the Mellin transform (Sneddon, 1951), and $M_{a\delta} \sim M_{d\delta}$ of Step 3 are functions involving the wedge angles, elasticity constants (Young's modulus and Poisson's ratio) and the root p_j. In eqns (1) and (2), the stress intensities K_{hj}, K_{hpa}, K_{hg} and K'_{hg} of each solution non-dimensionalized by $E_2\alpha_2\Delta T/(1+\nu_2)$ can be written as

$$K_{hj} = \bar{K}_{hj}\left(n_1\frac{\alpha_1}{\alpha_2} - n_2\right)\text{etc.} \quad (7)$$

where $\bar{K}_{hj}$ is an independent function of the thermal expansion coefficient.

3. THEORETICAL RESULTS

In this section, the relation between the stress intensity K_{hj} and the bonded wedge angle in a metal/ceramics composite under thermal loading is examined in plane strain condition. The bonded structure of the Cu/Si_3N_4 composite composed of three-quarters planes with material properties as shown in Fig. 2 is analyzed. A uniform negative temperature change $-\Delta T$ is assumed to act on the whole of the structure. Such a situation occurs during soldering of a metal/ceramics composite.

3.1. *Distribution of stress intensity*

The variations of roots p_j of the eigen equation with the wedge angle φ_1 of material 1 are plotted in Fig. 3. The roots noted here are only concerned with the stress singularity. The roots in the cases of $\varphi_1 = 0°$ and 270° agree with those in a free-free single wedge for a wedge angle of 270° given by Williams (1952). Varying the wedge angle φ_1 from 0° to 270°, two roots p_1 and p_2 yielding the singular solution of type r^{p-1} occur, where the second root p_2 is a double root at $p_2 = 1$ in $\varphi_1 = 97.20°$ and 120.24°, i.e. the singular solution of type $\log r$ occurs. Also, the solution for p_2 exhibits no singularity in the range of $97.20° < \varphi_1 < 120.24°$. The solution for the first root p_1 yielding the dominant factor on the stress field near the apex gives the singular solution of type r^{p-1} for all values of φ_1. Figures 4 and 5 show the distributions of stress intensity against angle θ of roots p_1 and p_2 in the cases of $\varphi_1 = 45°$ and 180°, respectively, where F_1 and F_2 indicate the free surface, and B_{12} and CL indicate the interface ($\theta = 0°$), and $\gamma = 0°$ ($-135° \leqslant \gamma \leqslant 135°$) as shown in Fig. 2. $\bar{K}_{hj}$ shown in these figures is the independent function of the thermal expansion coefficient as shown in eqn (7). It is found from Fig. 4 that the signs (tension and compression) of stress intensity for p_1 in $\varphi_1 = 45°$ are reversed to those in $\varphi_1 = 180°$ for each stress component ($rr, r\theta, \theta\theta$). The form of the distribution as shown in $\varphi_1 = 45°$ is referred to as Style 1, and that in $\varphi_1 = 180°$ as Style 2. Also, $K_{\theta\theta 1}$ attains a maximum tension in Style 1 and compression in Style 2 at *ca.* $\gamma = 0°(CL)$, where $\gamma = (\varphi_1 - 135°) + \theta$ from the relation illustrated in Fig. 2. In Fig. 5, the distributions of the stress intensity for p_2 in $\varphi_1 = 45°$ are reversed to those in $\varphi_1 = 180°$. The form of the distribution in $\varphi_1 = 45°$ is

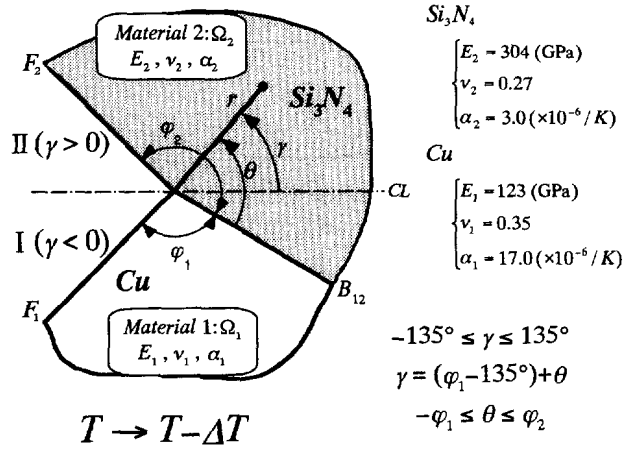

Fig. 2. Cu/Si_3N_4 composite in three-quarter planes under thermal loading.

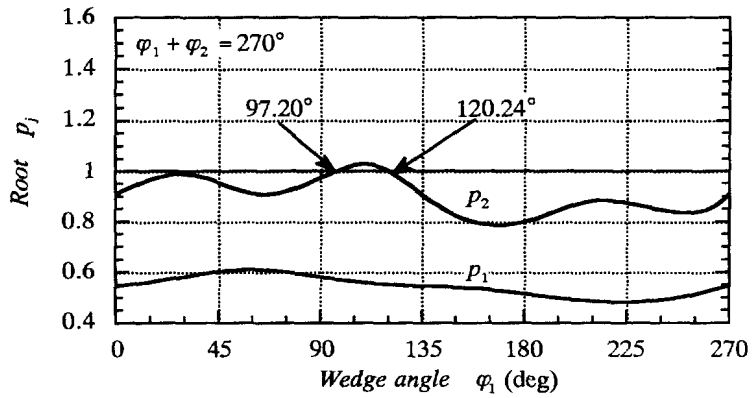

Fig. 3. Variations of roots p_j of the eigen equation concerned with stress singularity against wedge angle φ_1 of material 1.

referred to as Style 3 and that in $\varphi_1 = 180°$ as Style 4. Also, it is found that $K_{\theta\theta 2}$ attains a maximum tension and compression near $\gamma = \pm(\varphi_1+\varphi_2)/5$, as well as $K_{r\theta 2}$ near $\gamma = 0°$, $\pm(\varphi_1+\varphi_2)/3$ in both Style 3 and 4.

In these results, the distribution of the stress intensity K_{hj} is divided into two forms of Style 1 and 2 for p_1 and Style 3 and 4 for p_2. We expect that the stress intensity K_{hj} becomes zero regardless of angle θ at a bonded wedge angle where the distribution form of the intensity varies from Style 1 to 2 for p_1 and from Style 3 to 4 for p_2.

3.2. *Bonded wedge angle satisfying* K = 0

The stress intensity K_{hj} for root p_j is defined as

$$K_{rrj}(p_j,\theta)|_\delta = -\left[\frac{d^2}{d\theta^2}+(p_j+1)\right]K_{Fj}(p_j,\theta)|_\delta$$

$$K_{r\theta j}(p_j,\theta)|_\delta = p_j\frac{d}{d\theta}K_{Fj}(p_j,\theta)|_\delta$$

$$K_{\theta\theta j}(p_j,\theta)|_\delta = -p_j(p_j+1)K_{Fj}(p_j,\theta)|_\delta, \tag{8}$$

where the function $K_{Fj}(p_j,\theta)$ is given by

$$K_{Fj}(p_j,\theta)|_\delta = \left(n_1\frac{\alpha_1}{\alpha_2}-n_2\right)\bar{K}_{Fj}(p_j,\theta)|_\delta = \left(n_1\frac{\alpha_1}{\alpha_2}-n_2\right)\frac{M(p_j,\theta)|_\delta}{p_j(p_j-1)\dfrac{d}{dp}S|_{p=p_j}} \tag{9}$$

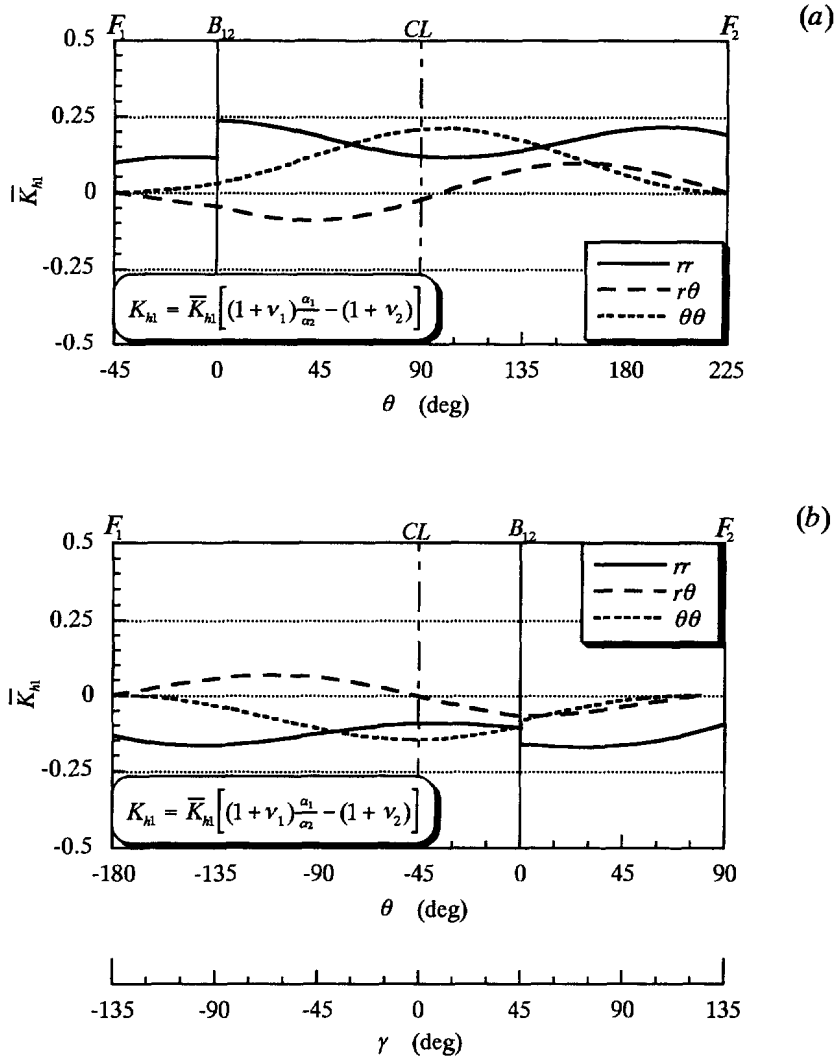

Fig. 4. Distributions of stress intensity $\bar{K}_{h1}$ independent of the thermal expansion coefficient for root (a) $p_1 = 0.6022$ in $\varphi_1 = 45°$ and (b) $p_1 = 0.5148$ in $\varphi_1 = 180°$.

with

$$M(p_j, \theta)\,|_\delta = -M_{a\delta}(p_j)\sin[(p_j+1)\theta] + M_{b\delta}(p_j)\cos[(p_j+1)\theta] - M_{c\delta}(p_j)\sin[(p_j-1)\theta] + M_{d\delta}(p_j)\cos[(p_j-1)\theta], \quad (10)$$

where, $\delta(=1,2)$ represents each region number. Also, $M_{a\delta} \sim M_{d\delta}$ are functions involving the wedge angles, Dundurs parameters and the root p of the eigen equation. Hence, the stress intensity K_{hj} for each component becomes zero in all regions (i.e. regardless of angle θ) according to the function $K_{Fj} = 0$, i.e. $M_{a\delta} = M_{b\delta} = M_{c\delta} = M_{d\delta} = 0$.

Figure 6 shows the relationship between the function K_{F1} for the root p_1 at $\gamma = 0°(CL)$ and the wedge angle φ_1, where the function $\bar{K}_{F1}$ is independent of the thermal expansion coefficient. In this result, $\bar{K}_{F1}$ is positive in the range $0° < \varphi_1 < 146.50°$, negative in $146.50° < \varphi_1 < 270°$ and equal to zero at $\varphi_1 = 146.50°$. Therefore, the distribution of the stress intensity K_{h1} represents Style 1 in the range $0° < \varphi_1 < 146.50°$ and Style 2 in $146.50° < \varphi_1 < 270°$, and K_{h1} becomes zero regardless of angle θ at the angle $\varphi_1 = 146.50°$ where the distribution varies from Style 1 to 2. Furthermore, $\bar{K}_{F1}$ becomes zero at $\varphi_1 = 0°$ and 270°, i.e. a free-free single wedge for 270°.

Figure 7 shows the variation of function $\bar{K}_{F2}$ for the root p_2 at $\gamma = 54°$ with the wedge angle φ_1. As seen from Fig. 7, the function $\bar{K}_{F2}$ becomes zero at $\varphi_1 = 85.60°$ and 195.10°,

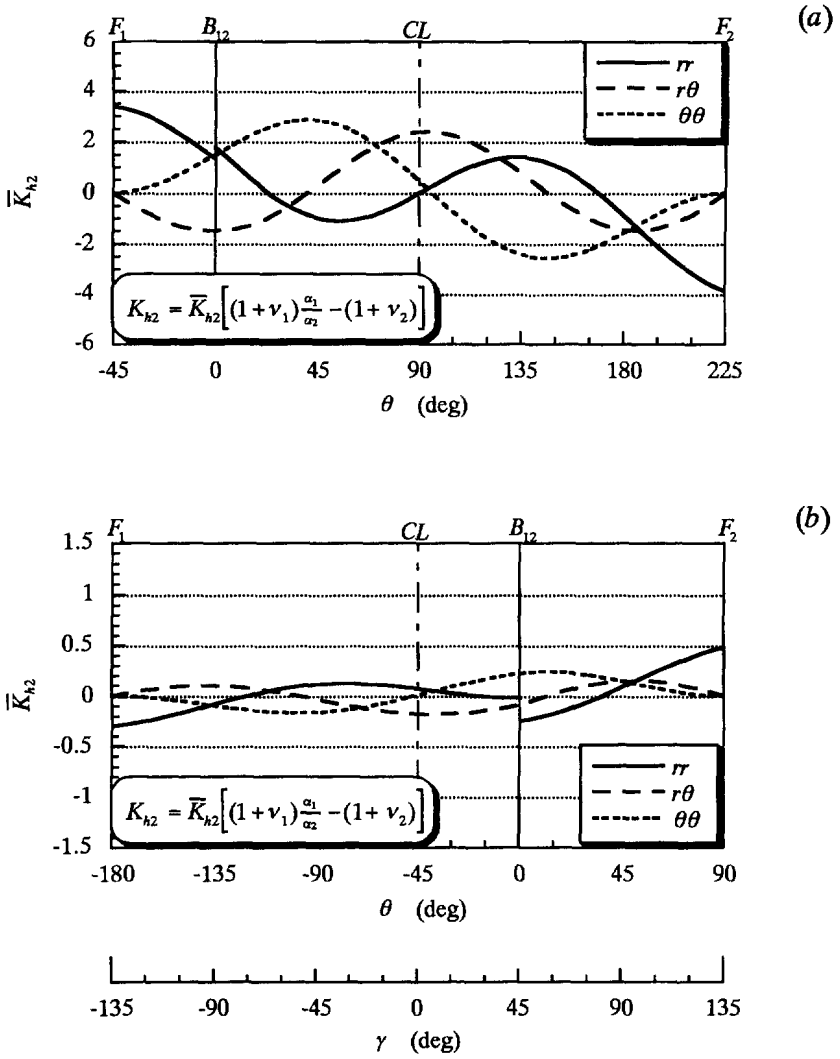

Fig. 5. Distributions of stress intensity $\bar{K}_{h2}$ independent of the thermal expansion coefficient for root (a) $p_2 = 0.9536$ in $\varphi_1 = 45°$ and (b) $p_2 = 0.7986$ in $\varphi_1 = 180°$.

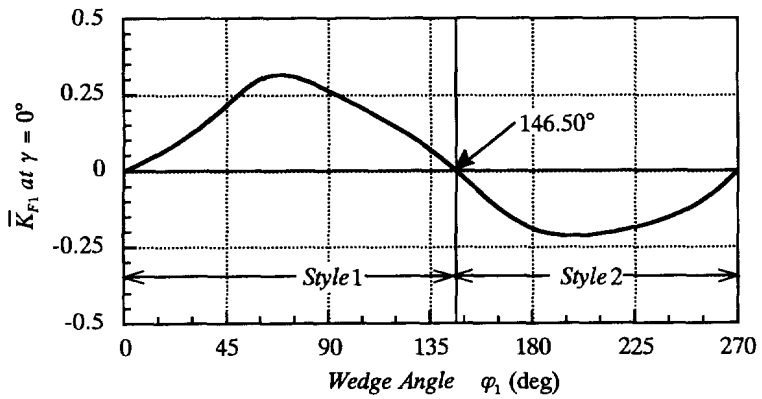

Fig. 6. Relationship between function $\bar{K}_{F1}$ for root p_1 at $\gamma = 0°$ and wedge angle φ_1 of material 1.

and larger as the angle φ_1 approaches the bonded wedge geometry with logarithmic singularity, i.e. $\varphi_1 \to 97.20°$ and $\varphi_1 \to 120.24°$. It is found that the sign of $\bar{K}_{F2}$ is reversed at these wedge angles. Consequently, the distribution of the stress intensity K_{h2} represents Style 3 in $0° < \varphi_1 < 85.60°$, $97.20° < \varphi_1 < 120.24°$ and $195.10° < \varphi_1 < 270°$, and Style 4 in

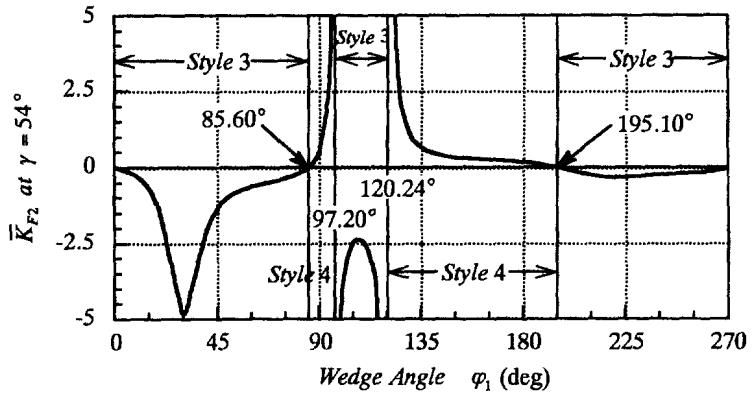

Fig. 7. Relationship between function $\bar{K}_{F2}$ for root p_2 at $\gamma = 54°$ and wedge angle φ_1 of material 1.

$85.60° < \varphi_1 < 97.20°$ and $120.24° < \varphi_1 < 195.10°$. Furthermore, $\bar{K}_{F2}$ becomes zero at $\varphi_1 = 0°$ and 270°.

4. DISCUSSION

4.1. *Results of analysis*

It is found from Figs 4–7 that the distribution of the stress intensity K_{hj} is divided into two forms of Style 1 and 2 for p_1, and Style 3 and 4 for p_2 at the angle, φ_1, yielding the conditions of $K_{hj} = 0$ and $p \to 1$ (a double root of the eigen equation). The first condition $K_{hj} = 0$ is derived from the numerator $M(p_j, \theta)$ in eqn (9) and the second $p \to 1$ from the eigen equation in eqn (4). The magnitude of the stress intensity K_{hj} strongly depends on the value of the first derivative of the eigen equation, i.e. $(dS/dp)_{p=pj}$. Figure 8 shows $(dS/dp)_{p=pj}$ and $(dS/dp)_{p=1}$ against the wedge angle φ_1. It can be seen that the absolute values of $(dS/dp)_{p=p1}$ compare largely with those of $(dS/dp)_{p=p2}$. Therefore, the magnitude of K_{h1} for root p_1 is small in comparison with that of K_{h2} for p_2 (Figs 4 and 5). The value of $(dS/dp)_{p=p1}$ does not change the sign of K_{h1}, since it is negative for all values of φ_1. Incidentally, the value of $(dS/dp)_{p=p2}$ is positive in the range $0° \leqslant \varphi_1 < 97.20°$ and $120.2° < \varphi_1 \leqslant 270°$ (singularity of type r^{p-1}), negative in the range $97.20° < \varphi_1 < 120.24°$ (no singularity) and zero at $\varphi_1 = 97.20°$ and 120.24° (logarithmic singularity). Hence, $(dS/dp)_{p=p2}$ affects the change of sign of K_{h2}. Also, the stress intensity K_{h2} approaches infinity as $\varphi_1 \to 97.20°$ and $\varphi_1 \to 120.24°$ (Fig. 7), because the values of $(dS/dp)_{p=p2}$ then approach zero. The particular solution K_{hpa} [Munz *et al.* (1993b) called this solution the regular stress term] also approaches infinity as $\varphi_1 \to 97.20°$ and $\varphi_1 \to 120.24°$ [i.e. $(dS/dp)_{p=1}$], where it always has the opposite sign as K_{h2} because $(dS/dp)_{p=p2}$ and $(dS/dp)_{p=1}$ have the opposite sign. Therefore, $K_{h2}/K_{hpa} \to -1$ for $p \to 1$. This characteristic agrees with that obtained by Munz and Yang (1993a), and Munz *et al.* (1993b).

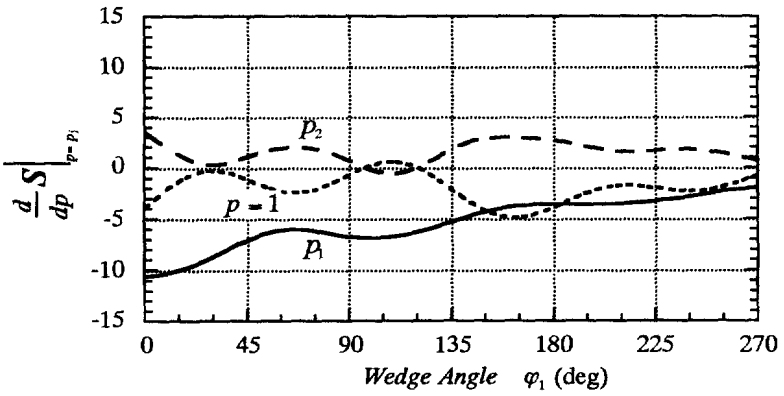

Fig. 8. First derivative dS/dp of roots p_1, p_2 and $p = 1$ with wedge angle φ_1 of material 1.

Furthermore, in the present analysis, the distribution of stress intensity for dissimilar materials under cooling was examined and that under heating is obtained by reversing the signs of results for the present analysis.

4.2. *Relation with* K = 0 *of wedge angle* φ_1 and total angle $\varphi_1+\varphi_2$

The singular solution $K_{hj}r^{p_j-1}$ can disappear under combinations of materials yielding $K_{hj}=0$, even if root p_j of the eigen equation exists in $0<\mathrm{Re}(p)<1$. Figure 9(a) shows the relationship yielding $K_{h1}=0$ between the wedge angle φ_1 and the total angle $\varphi_1+\varphi_2$ of the bonded wedge in the Cu/Si_3N_4 composite under thermal loading. Figure 9(b) shows the variations of the corresponding root p_1 with the total angle $\varphi_1+\varphi_2$. The bonded wedge angle, $\varphi_1+\varphi_2$, yielding $K_{h1}=0$ exists in the range of $163^\circ \leqslant \varphi_1+\varphi_2 \leqslant 337^\circ$, but does not exist in the ranges of $\varphi_1+\varphi_2<163^\circ$ and $\varphi_1+\varphi_2>337^\circ$, because the corresponding root p_1 is then a complex one $p(=\xi\pm i\eta)$. When $p=\xi\pm i\eta$, the intensity is separated into the real part $K_{h\xi}$ and imaginary part $K_{h\eta}$, and the bonded wedge angle yielding simultaneously $K_{h\xi}=0$ and $K_{h\eta}=0$ then does not exist. Also, it is found from Fig. 9(a) that the bonded angle yielding $K_{h1}=0$ exists in the range of $\varphi_1>(\varphi_1+\varphi_2)/2$ when $G_1<G_2$ and in that of $\varphi_1<(\varphi_1+\varphi_2)/2$ when $G_1>G_2$. In the range $170^\circ \leqslant \varphi_1+\varphi_2 \leqslant 305^\circ$, the relationship between φ_1 and $\varphi_1+\varphi_2$ can be expressed by the approximate equation: $\varphi_1=0.464(\varphi_1+\varphi_2)+21.766$. In Fig. 9(b), the corresponding root p_1 is within $1.3507 \geqslant p_1 \geqslant 0.5057$, where p_1 is larger than 1 (no singularity) in $\varphi_1+\varphi_2<180^\circ$ and smaller than 1 (singularity of type r^{p-1}) in

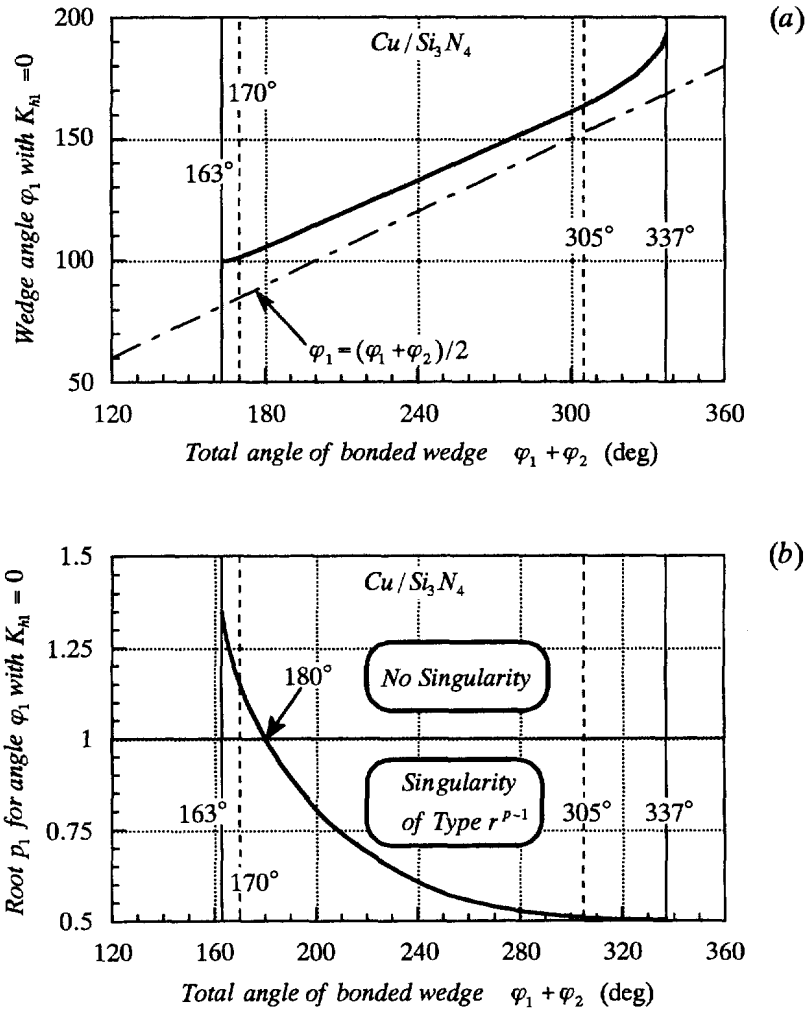

Fig. 9. (a) Relationship yielding $K_{h1}=0$ between the wedge angle φ_1 of material 1 and the total angle $\varphi_1+\varphi_2$ of the bonded wedge and (b) variations of the corresponding root p_1, in the Cu/Si_3N_4 composite under thermal loading.

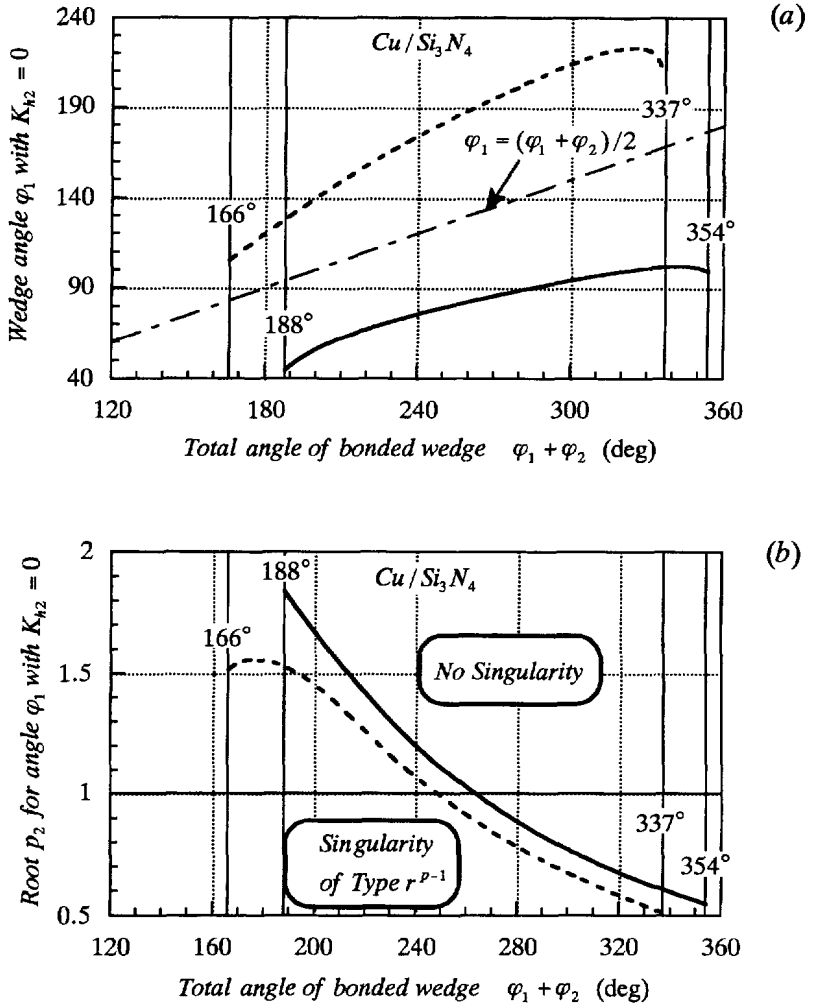

Fig. 10. (a) Relationship yielding $K_{h2} = 0$ between the wedge angle φ_1 of material 1 and the total angle $\varphi_1 + \varphi_2$ of the bonded wedge and (b) variations of the corresponding root p_2, in the Cu/Si_3N_4 composite under thermal loading.

$\varphi_1 + \varphi_2 > 180°$, i.e. the root p_1 for $\varphi_1 + \varphi_2 = 180°$ gives a boundary of singularity and no singularity.

Figure 10(a) shows the relationship yielding $K_{h2} = 0$ between φ_1 and $\varphi_1 + \varphi_2$ for the Cu/Si_3N_4 composite under thermal loading and Fig. 10(b) shows the variations of the corresponding root p_2 with the total angle $\varphi_1 + \varphi_2$. The wedge angle φ_1 yielding $K_{h2} = 0$ exists one by one in $\varphi_1 > (\varphi_1 + \varphi_2)/2$ and in $\varphi_1 < (\varphi_1 + \varphi_2)/2$, respectively. One exists in the range $188° \leqslant \varphi_1 + \varphi_2 \leqslant 354°$ and another in $166° \leqslant \varphi_1 + \varphi_2 \leqslant 337°$. A slope against φ_1 yielding $K_{h2} = 0$ against $\varphi_1 + \varphi_2$ existing in $\varphi_1 > (\varphi_1 + \varphi_2)/2$ is larger than 1/2 and that in $\varphi_1 < (\varphi_1 + \varphi_2)/2$ is smaller than 1/2. The corresponding root p_2 is within $1.8400 \geqslant p_2 \geqslant 0.5472$ and $1.5515 \geqslant p_2 \geqslant 0.5134$, respectively, and the root corresponding to the bonded geometry yielding $K_{h2} = 0$ existing in $\varphi_1 > (\varphi_1 + \varphi_2)/2$ is small in comparison with that existing in $\varphi_1 < (\varphi_1 + \varphi_2)/2$. Also, the ranges with $\varphi_1 + \varphi_2$ yielding $K_{h2} \neq 0$ exist, where the corresponding root p_2 is then a complex one.

4.3. *Classification of distribution on* K

The distributions of the stress intensities K_{h1} and K_{h2} are categorized on the $\varphi_1 + \varphi_2$–φ_1 plane from results denoted by (a) in Figs 9 and 10. The distributions of K_{h1} and K_{h2} are classified into Styles 1 and 2 for K_{h1} and Styles 3 and 4 for K_{h2}, respectively (Fig. 11). Figure 11 shows the classification for dissimilar materials under cooling. On the other hand, the classification under heating is obtained by changing each Style shown in Fig. 11, such as

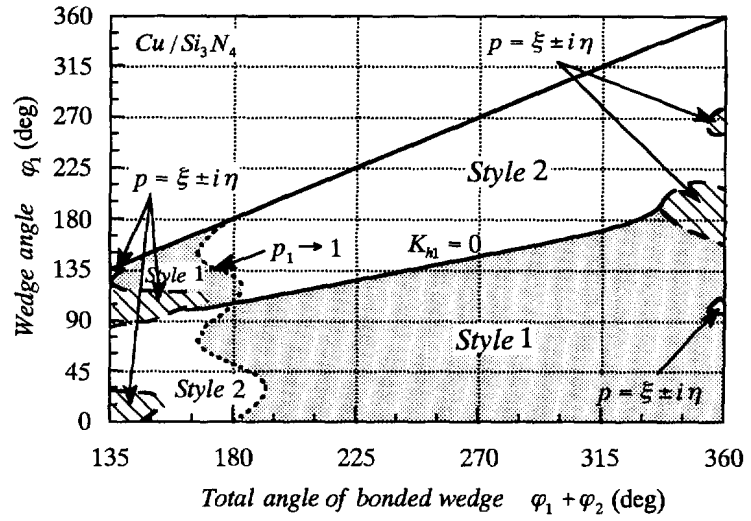

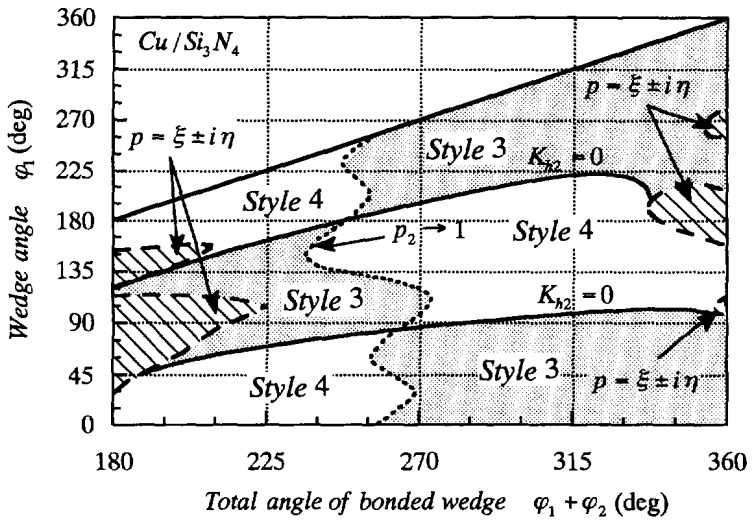

Fig. 11. Classification of the distribution on the stress intensity for (a) first root p_1 and (b) second root p_2 in the Cu/Si_3N_4 composite cooling.

Styles 1 and 3 under cooling changes into Styles 2 and 4 under heating, respectively. It is found from Fig. 11 that the distributions alter from Style 1 to 2 and from Style 3 to 4, respectively, at conditions of $K_{hj} = 0$, $p_j \to 1$ (a double root at $p = 1$) and the complex root which depends on $K_{hj} = 0$. Two roots p_1 and p_2 are divided in $\mathrm{Re}(p) > 1$ (the left side of the $p_j \to 1$ line in Fig. 11) and $\mathrm{Re}(p) < 1$ (the right side of that) by the $p_j \to 1$ line. Therefore, the $K_{hj} = 0$ line and the region of the left side of $p_j \to 1$ line depicted in Fig. 11 indicate the disappearance conditions of stress singularity for each solution. Here, in the region between the right side of $p_1 \to 1$ and the left side of $p_2 \to 1$, root p_j existing in the range of $0 < \mathrm{Re}(p) < 1$ is only p_1; hence, the stress singularity then disappears if $K_{h1} = 0$. In the region of the right side of $p_2 \to 1$, two roots p_1 and p_2 exist in the range of $0 < \mathrm{Re}(p) < 1$; hence, the singularity then does not disappear even if $K_{h1} = 0$, because there is the singular solution for the second root p_2. However, the thermal stresses then become small because the singular solution for the first root p_1, yielding the most dominant factor on the stress field near the apex, disappears.

Also, K_{h1} and K_{h2} do not always represent the distributions of Styles 1 and 2 for K_{h1} and Styles 3 and 4 for K_{h2}. Those distributions differ from Styles 1–4 as the combinations of wedge angles approach the regions producing complex roots. In the case of $\varphi_1 + \varphi_2 \approx 360°$, the distribution styles of K_{h1} and K_{h2} for all the combinations of wedge

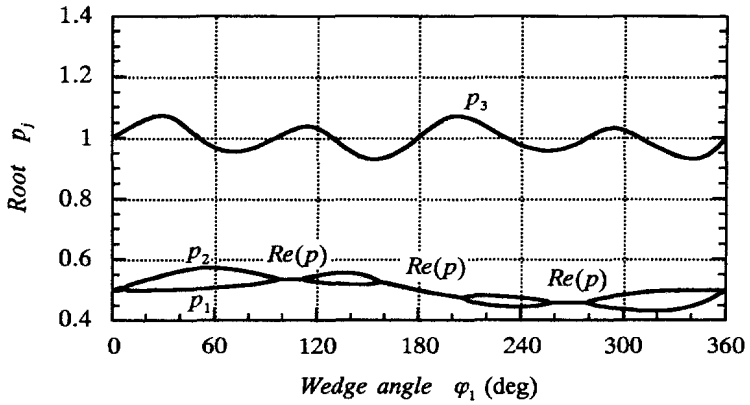

Fig. 12. Variations of root p_j against wedge angle φ_1 in the Cu/Si_3N_4 composite with $\varphi_1+\varphi_2 = 360°$.

angles differ from Style 1–4, because the values of roots p_1 and p_2 are then nearly equal (Fig. 12). Complex root occurs when two real roots combine with variations of wedge angles of materials and their mechanical properties, which has been clarified by many researchers (Inoue and Koguchi, 1996; Pageau *et al.*, 1994a; Hein and Erdogan, 1971; Fenner, 1976). Hence, when the values of two real roots p_1 and p_2 are almost equal, the distribution forms of stress intensity for these roots indicate the characteristic near the condition of $p = \xi \pm i\eta$. Furthermore, the magnitude of the stress intensity K_{hj} becomes larger as the combinations of wedge angles approach the conditions of $p_j \to 1$ and those of $p_j, p_{j+1} \to p = \xi \pm i\eta$. As mentioned previously, $K_{hj}/K_{hpa} \to -1$ for conditions of $p_j \to 1$. For conditions of p_j and $p_{j+1} \to p = \xi \pm i\eta$, when K_{hj} approaches infinity, the corresponding intensity $K_{h(j+1)}$ also approaches infinity, where $K_{h(j+1)}$ always has the opposite sign as K_{hj}; therefore $K_{hj}/K_{h(j+1)} \to -1$ for $p_j, p_{j+1} \to p = \xi \pm i\eta$.

4.4. *For other stress intensities*

The distribution of the stress intensity K_{h3} for the third root p_3 is also divided into two forms (Styles 5 and 6) with different signs for each stress component. Figure 13(a) and (b) show the distributions of K_{h3} for root $p_3 = 1.0330$ and 0.9310 in the case of the Cu/Si_3N_4 composite with $\varphi_1 = 120°$ and 150°, respectively, in the condition of $\varphi_1+\varphi_2 = 360°$ under cooling. The form of the distribution as shown in Fig. 13(a) is referred to as Style 5 and that in Fig. 13(b) as Style 6. The stress intensity $K_{\theta\theta 3}$ attains a maximum tension in Style 5 and compression in Style 6 near $\gamma = \pm(\varphi_1+\varphi_2)/4$, and a minimum in Style 5 and a maximum in Style 6 near $\gamma = 0°(CL)$. Moreover, the distribution of K_{h3} is nearly symmetrical with respect to $\gamma = 0°$.

The distribution of the particular solution K_{hpa} for $p = 1$ as expressed in eqn (1) can be perceived from K_{hj} for root p_j. Then, the distribution of K_{hpa} is represented by the distributions of K_{hj} for $p = p_j$ near the condition of $p = 1$. For example, it is found from Fig. 12 that the closest root to $p = 1$ is the third one p_3, regardless of φ_1 in the Cu/Si_3N_4 composite with $\varphi_1+\varphi_2 = 360°$. The distribution of K_{hpa} is then represented by Styles 5 and 6 (Fig. 14). As mentioned previously, the distribution form of K_{hpa} always has the opposite sign as that of K_{hj}. Also, the combinations of wedge angles and mechanical properties yielding $K_{hpa} = 0$ do not exist. Moreover, for the conditions of $K_{hj} = 0$, $p = \xi \pm i\eta$ and those close to those conditions, the distribution form of K_{hpa} differs from that of K_{hj}.

The distribution forms of the stress intensity K_{hg} of the singular solution of type $\log r$, as expressed in eqn (2) is represented by that of K_{hpa} near the condition of $p_j \to 1$, however, the distribution form of K'_{hg} for $p \to 1$ in eqn (2) differs from that of K_{hj}. Figure 15 shows the distributions of K_{hg} and K'_{hg} for the double root $p \to 1$ with $\varphi_1 = 129.2°$ in the Cu/Si_3N_4 composite formed from $\varphi_1+\varphi_2 = 360°$ under cooling. It is found from Fig. 15 that the distribution form of K_{hg} is represented by Style 5.

The distribution form of $K_{h\xi}$ and $K_{h\eta}$ for $p = \pm\xi i\eta$ represent similar forms to K_{hj} and $K_{h(j+1)}$ for p_j, p_{j+1} depending on the complex root. i.e. when $p = \xi \pm i\eta$ occurs by combining the two roots p_1 and p_2 against wedge angles of materials and their mechanical properties,

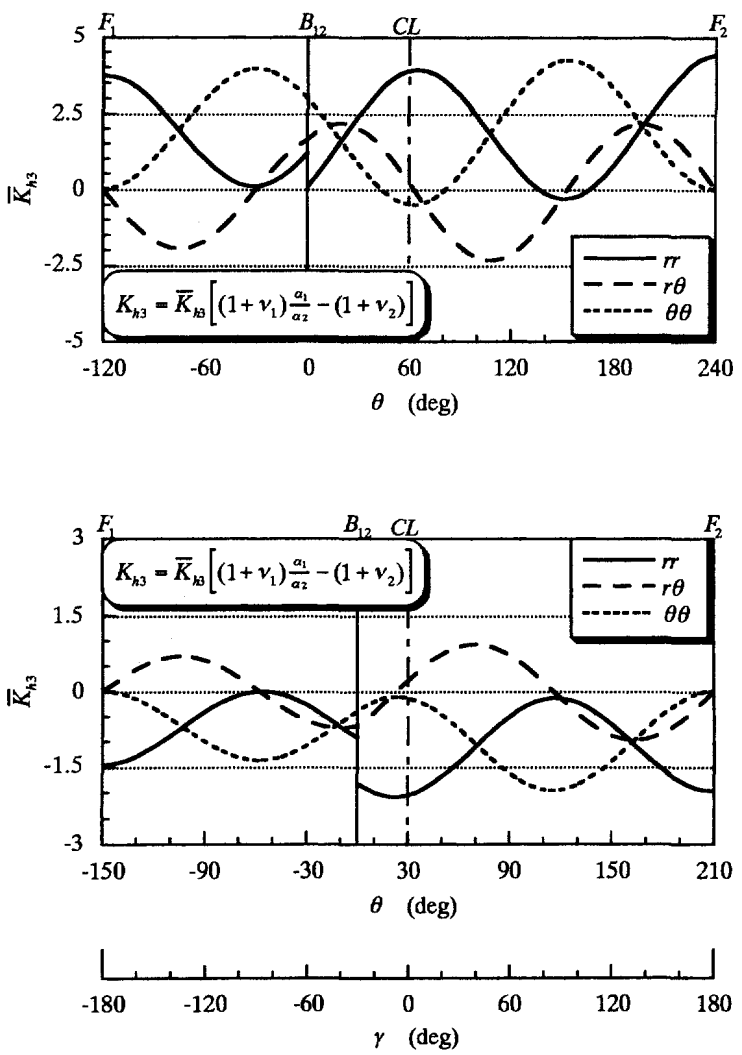

Fig. 13. Distributions of stress intensity $\bar{K}_{h3}$ independent of the thermal expansion coefficient for the third root (a) $p_3 = 1.0330$ when $\varphi_1 = 120°$ and (b) $p_3 = 0.9310$ when $\varphi_1 = 150°$, in the Cu/Si_3N_4 composite with $\varphi_1 + \varphi_2 = 360°$ under cooling.

the distribution forms of $K_{h\xi}$ and $K_{h\eta}$ are expressed by Styles 1–4, and when it occurs by combining p_2 and p_3 against those, $K_{h\xi}$ and $K_{h\eta}$ by Styles 3–6. Also, $K_{h\xi}$ and $K_{h\eta}$ are larger as complex root $p = \xi \pm i\eta$ approaches the condition changing into a real root with wedge angles of materials and their mechanical properties, because the values of $(dS/dp)_{p=\xi\pm i\eta}$ approach zero.

4.5. *Discussion by FEM*

The distribution of the thermal stresses near the apex is examined by FEM (MARC). For Cu/Si_3N_4 under $\Delta T = -500$ K, two geometries (Fig. 16) are used in plane strain condition (see Fig. 2 for the material data). The stress intensity theoretically becomes $K_{h1} = 0$ when $\varphi_1 = 118.87°$ (then, $p_1 = 0.7394$) for $\varphi_1 + \varphi_2 = 210°$, and $K_{h1} = 0$ when $\varphi_1 = 146.50°$ ($p_1 = 0.5410$) and $K_{h2} = 0$ when $\varphi_1 = 85.60°$ ($p_2 = 0.9527$) and $195.10°$ ($p_2 = 0.8437$) for $\varphi_1 + \varphi_2 = 270°$. From Fig. 11, the classification of distribution for K_{h1} and K_{h2} is perceived, and it is found that root p_j existing in the range of $0 < \mathrm{Re}(p) < 1$ is only p_1 for $\varphi_1 + \varphi_2 = 210°$, and p_1 and p_2 for $\varphi_1 + \varphi_2 = 270°$.

In the case of $\varphi_1 + \varphi_2 = 210°$, combinations (φ_1, φ_2) of the four bonded wedge are chosen as follows:

$$(36°, 174°) \to p_1 = 0.8596, \quad (84°, 126°) \to p_1 = 0.7300$$

$$(114°, 96°) \to p_1 = 0.7334, \quad (144°, 66°) \to p_1 = 0.7293.$$

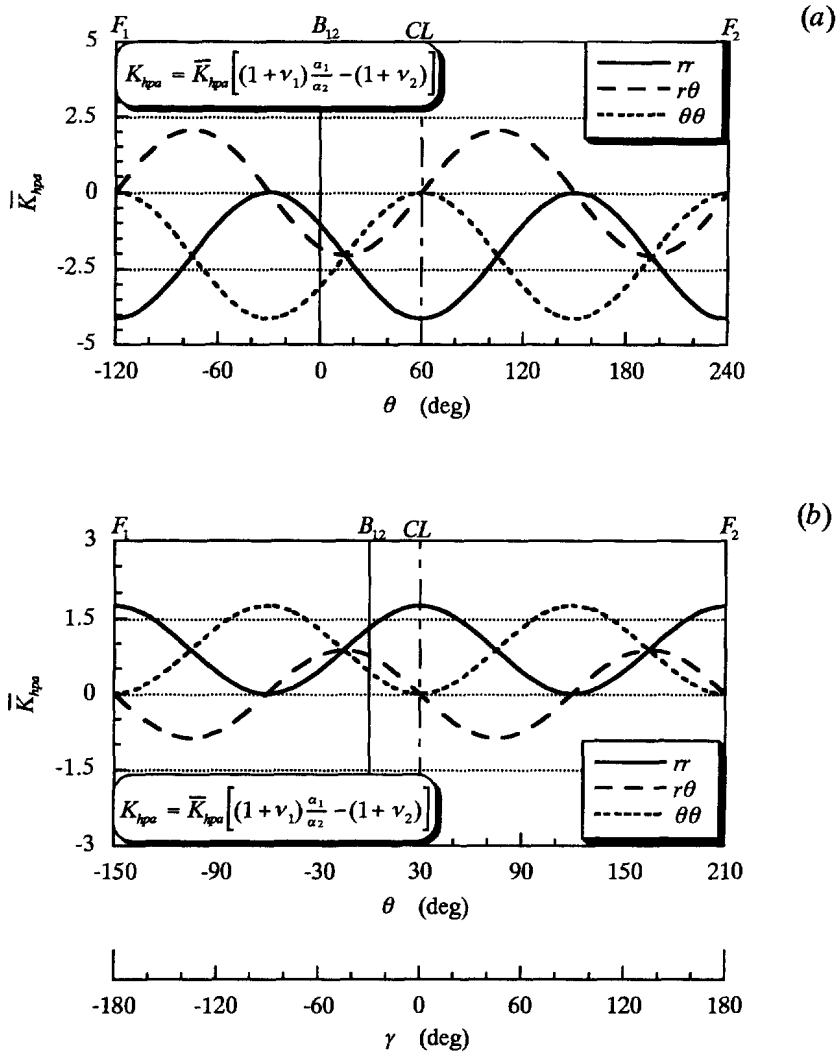

Fig. 14. Distributions of stress intensity $\bar{K}_{hpa}$ independent of the thermal expansion coefficient for root $p = 1$ (a) when $\varphi_1 = 120°$ and (b) when $\varphi_1 = 150°$, in the Cu/Si_3N_4 composite with $\varphi_1 + \varphi_2 = 360°$ under cooling.

The distributions for θ-direction stress $\sigma_{\theta\theta}$ near the apex, calculated using the FEM, are shown in Fig. 17. Furthermore, the distribution of the stress for a point at $\rho = r/a = 1.2821 \times 10^{-4}$ is plotted. It can be seen from Fig. 17 that the stress distribution is expressed by Style 1 when the combination of the bonded wedge is $(36°, 174°)$ and $(84°, 126°)$, and by Style 2 when that of the bonded wedge is $(144°, 126°)$. These results agree with the classification of the distribution of the intensity K_{h1} for the singular solution yielding the dominant factor on the stress field near the apex, as shown in Fig. 11(a). Also, the stress in the case of $(114°, 96°)$ compares insignificantly with that in the other cases, because the combination of the bonded wedge angle is near $(118.87°, 91.13°)$ yielding $K_{h1} = 0$.

In the case of $\varphi_1 + \varphi_2 = 270°$, combinations (φ_1, φ_2) of the four bonded wedge are considered as follows:

$$(30°, 240°) \to p_1 = 0.5819, p_2 = 0.9895, \quad (60°, 210°) \to p_1 = 0.6111, p_2 = 0.9102$$

$$(144°, 126°) \to p_1 = 0.5419, p_2 = 0.8525, \quad (198°, 72°) \to p_1 = 0.4951, p_2 = 0.8533.$$

The distributions for the stress $\sigma_{\theta\theta}$ near the apex ($\rho = r/a = 1.2821 \times 10^{-4}$), calculated using the FEM are shown in Fig. 18. It can be seen that the stress distribution is expressed by

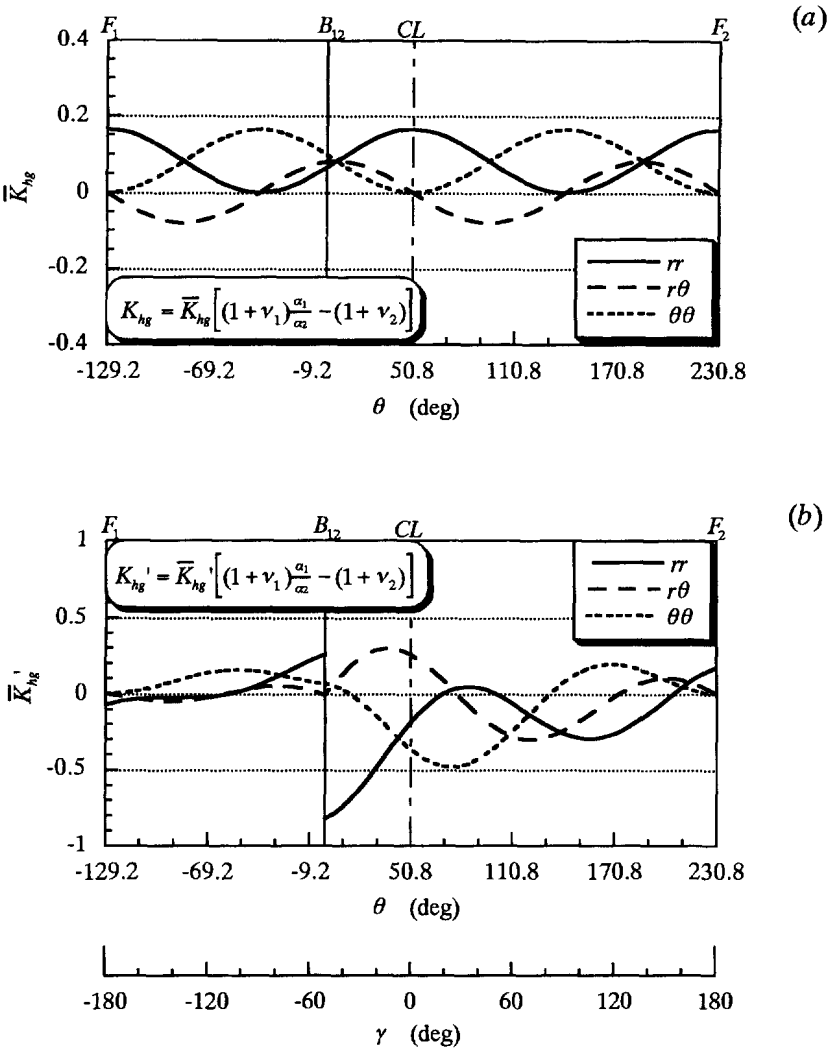

Fig. 15. Distributions of stress intensity (a) $\bar{K}_{hg}$ and (b) $\bar{K}'_{hg}$ independent of the thermal expansion coefficient for the double root $p \to 1.00$, in the Cu/Si_3N_4 composite with $\varphi_1 + \varphi_2 = 360°$ under cooling.

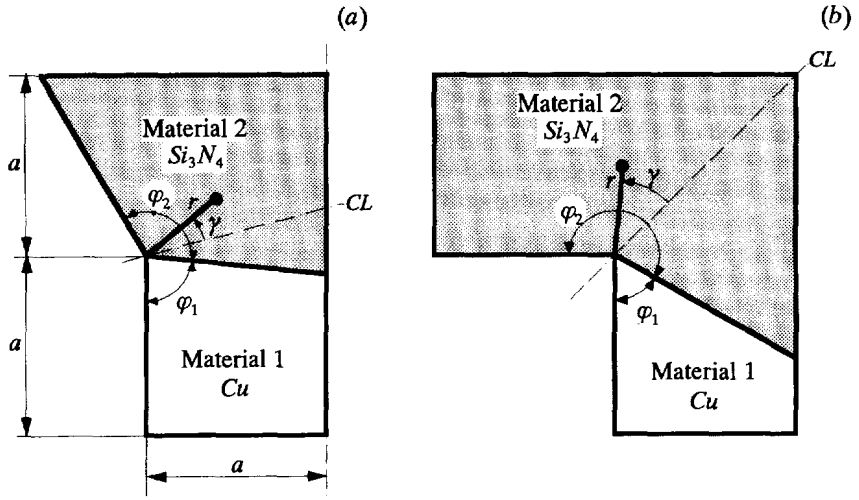

Fig. 16. The bonded structure of the Cu/Si_3N_4 composite in (a) $\varphi_1 + \varphi_2 = 210°$ and (b) $\varphi_1 + \varphi_2 = 270°$.

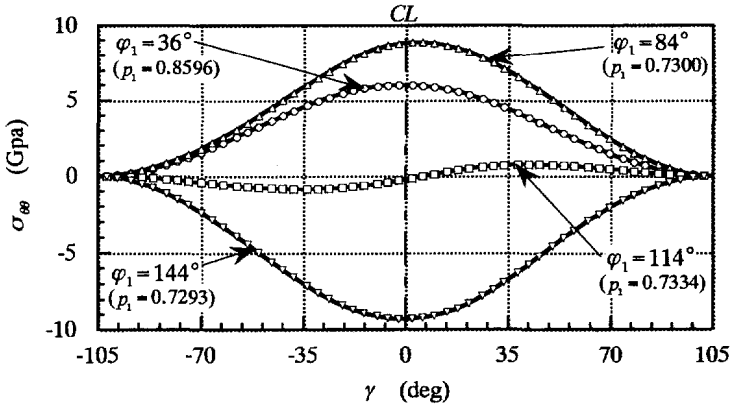

Fig. 17. Distributions of the thermal stress $\sigma_{\theta\theta}$ at $\rho = 1.1281 \times 10^{-4}$ for $\varphi_1 = 36°$, 84°, 114° and 144° in case of $\varphi_1 + \varphi_2 = 210°$, where $\gamma = (\varphi_1 - 105°) + \theta$.

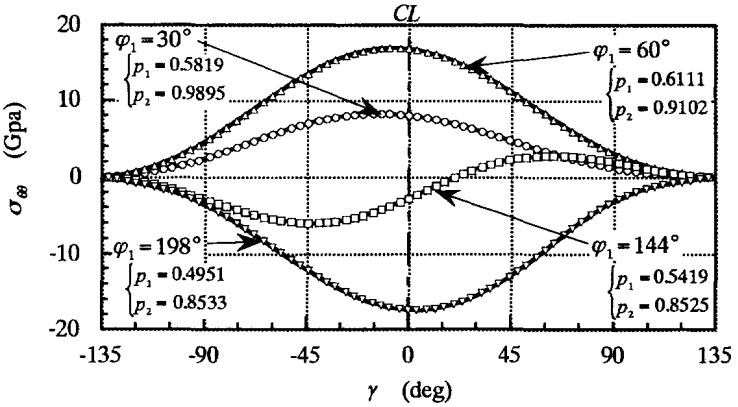

Fig. 18. Distributions of the thermal stress $\sigma_{\theta\theta}$ at $\rho = 1.1281 \times 10^{-4}$ for $\varphi_1 = 30°$, 60°, 144° and 198° in case of $\varphi_1 + \varphi_2 = 270°$, where $\gamma = (\varphi_1 - 135°) + \theta$.

Style 1 when the bonded wedge angle is (30°, 240°) and (60°, 210°), and Style 2 when it is (198°, 72°). These results agree with the distribution of the intensity K_{h1} shown in Fig. 11(a). Also, the stress distribution is represented by Style 4 when the bonded wedge angle is (144°, 126°), because the combination of the bonded wedge angle is near (146.50°, 123.50°) yielding $K_{h1} = 0$. Hence, the thermal stresses are then dominated by the singular solution $K_{h2}\rho^{p_2-1}$ for the second root p_2.

5. CONCLUSIONS

Characteristics of thermal stresses near the apex in dissimilar materials under thermal loading were investigated theoretically and numerically. For the Cu/Si_3N_4 composite, the relation between the intensity K_{hj} of the stress field and bonded wedge angle was examined in detail. Moreover, classification of the distribution of the stress intensity K_{hj} was shown on the $\varphi_1 + \varphi_2$–φ_1 plane. The contents in the present paper are summarized as follows.

(1) The distribution of the stress intensity against angle φ_1 is divided into the forms of Styles 1 and 2 for K_{h1}, Styles 3 and 4 for K_{h2} and Styles 5 and 6 for K_{h3}. The distribution form of each Style is illustrated in the Appendix. The boundary of the wedge angle φ_1, varying from Styles 1, 3 and 5 to Styles 2, 4 and 6 in the distribution, is obtained from the conditions of $K_{hj} = 0$, $p_j \to 1$ and $p = \xi \pm i\eta$ concerning $K_{hj} = 0$. Also the distribution forms of K_{hj} differ from each Style near the conditions of $p = \xi \pm i\eta$.

(2) There are combinations of wedge angles of materials and their mechanical properties for which the stress intensity K_{hj} is zero regardless of angle θ. The singular solutions can disappear by following the combinations satisfying the condition of $K_{hj} = 0$, even if root p_j of an eigen equation exists in the range of $0 < \mathrm{Re}(p) < 1$.

(3) The bonded wedge angle yielding $K_{h1} = 0$ for the first root p_1 exists in $\varphi_1 > \varphi_2$ when $G_1 < G_2$ and in $\varphi_1 < \varphi_2$ when $G_1 > G_2$. The wedge angle yielding $K_{h2} = 0$ for the second root p_2 exists one by one in $\varphi_1 > \varphi_2$ and in $\varphi_1 < \varphi_2$ regardless of stiffness ratio k_{12} $(=G_1/G_2)$, respectively.
(4) When root p is a complex number $p = \xi \pm i\eta$, the intensity K_{hj} is separated into a real part $K_{h\xi}$ and an imaginary one $K_{h\eta}$. Both $K_{h\xi}$ and $K_{h\eta}$ do not become simultaneously zero for all the bonded wedge geometries.
(5) The distribution form of the particular solution K_{hpa} is represented by the opposite sign of the distributions of K_{hj} for $p = p_j$ near the condition of $p = 1$, however, the combinations of wedge angles of materials and their mechanical properties yielding $K_{hpa} = 0$ do not exist. Moreover, for the conditions of $K_{hj} = 0$, $p = \xi \pm i\eta$ and those close to those conditions, the distribution form of K_{hpa} differs from that of K_{hj}. Furthermore, the distribution of K_{hg} for $p \to 1$ is represented by that of K_{hpa} for $p = 1$ near the condition of $p \to 1$.

Acknowledgement—This research was performed by Grant-in-Aid for JSPS Fellows under appointment to Research Fellow of the Japan Society for the Promotion of Science in JSPS Research Fellowships for Young Scientists.

REFERENCES

Blanchard, J. P. and Ghoniem, N. M. (1989) An eigenfunction approach to singular thermal stresses in bonded strips. *Journal of Thermal Stresses* **12,** 501–527.
Bogy, D. B. (1970). On the problem of edge-bonded elastic quarter-planes loaded at the boundary. *International Journal of Solids and Structures* **6,** 1287–1313.
Bogy, D. B. (1971a). Two-edge bonded elastic wedges of different materials and wedge angles under surface tractions. *Journal of Applied Mechanics* **38,** 377–386.
Bogy, D. B. (1971b). On the plane elastostatic problem of a loaded crack terminating at a material interface. *Journal of Applied Mechanics* **38,** 911–918.
Cook, T. S. and Erdogan, F. (1972). Stresses in bonded materials with a crack perpendicular to the interface. *International Journal of Engineering Science* **10,** 677–697.
Dundurs, J. (1969). Discussion of edge-bonded dissimilar orthogonal elastic wedges under normal and shear loading. *Journal of Applied Mechanics* **36,** 650–652.
Fenner, D. N. (1976). Stress singularities in composite materials with an arbitrarily oriented crack meeting an interface. *International Journal of Fracture Mechanics* **12,** 705–721.
Hein, V. L. and Erdogan, F. (1971). Stress singularities in a two-material wedge. *International Journal of Fracture Mechanics* **7,** 317–330.
Inoue, T., Koguchi, H. and Yada, T. (1994). Analysis near the apex in three-phase bonded material with arbitrary wedge angles under normal surface loading on the surface (1st report, stress distribution in the stress fields with singularity of type $r^{-\lambda}$ and $\log r$). *Transactions of the Japanese Society for Mechanical Engineers (A)* (in Japanese) **60-578,** 2286–2292.
Inoue, T., Koguchi, H. and Yada, T. (1995). Solution of thermal stresses near apex in dissimilar materials by thermoelastic theory. *Transactions of the Japanese Society for Mechanical Engineers (A)* (in Japanese) **61-581,** 73–79.
Inoue, T. and Koguchi, H. (1996). Influence of the intermediate material on the order of the stress singularity in three-phase bonded structure. *International Journal of Solids and Structures* **33,** 399–417.
Koguchi, H., Inoue, T. and Yada, T. (1996). Stress singularity in three-phase bonded structure. *Journal of Applied Mechanics* **63,** 252–258.
Munz, D. and Yang, Y. Y. (1993a). Stress near the edge of bonded dissimilar materials described by two stress intensity factors. *International Journal of Fracture* **60,** 169–177.
Munz, D., Fett, T. and Yang, Y. Y. (1993b). The regular stress term in bonded dissimilar materials after a change in temperature. *Engineering Fracture Mechanics* **44,** 185–194.
Pageau, S. S., Joseph, P. F. and Biggers, S. B. Jr (1994a). The order of stress singularities for bonded and disbonded three-material junctions. *International Journal of Solids and Structures* **31,** 2979–2997.
Pageau, S. S., Joseph, P. F. and Biggers, S. B. Jr (1994b). Finite element analysis of anisotropic materials with singular inplane stress fields. *International Journal of Solids and Structures* **32,** 571–591.
Sneddon, I. N. (1951). *The Use of Integral Transforms*, McGraw-Hill, New York.
Williams, M. L. (1952). Stress singularities resulting from various boundary conditions in angular corners of plates in extension. *Journal of Applied Mechanics* **19,** 526–528.

APPENDIX

In this appendix, we exhibit the distribution forms of Style 1–6 for each stress component $(rr, r\theta, \theta\theta)$. Tables A1 and A2 show the distributions of the stress intensity K_{rrj}, Table A3 shows those of $K_{r\theta j}$ and Table A4 those of $K_{\theta\theta j}$, in each Style for each root p_j, where $j = 1$, 2 and 3. Here, the distributions of K_{rrj} are illustrated for three cases where the interface B_{12} exists in the position of $\gamma = 0°$ and the stiffness ratio k_{12} is larger than 1 and smaller than 1 under the existing B_{12} at $\gamma = -(\varphi_1+\varphi_2)/3$, because the distribution forms of K_{rrj} vary somewhat against k_{12} and the position of B_{12} due to discontinuity on the interface.

Table A1. Distribution forms of the stress intensity K_{rrj} for each root p_j (in the case of existing interface at $\gamma = 0$)

Root	Distribution of stress intensity K_{rrj}
p_1	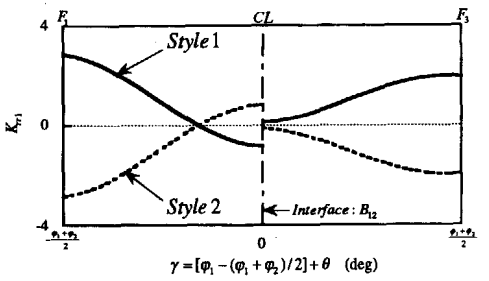
p_2	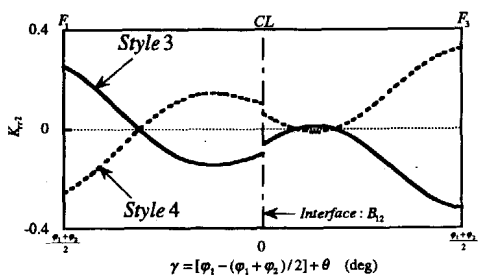
p_3	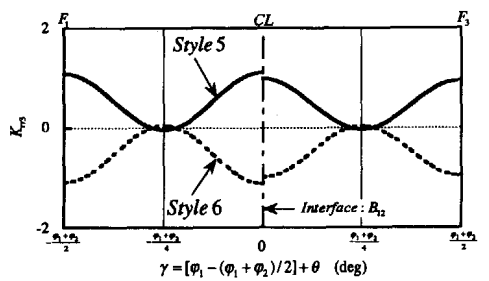

Table A2. Distribution forms of the stress intensity K_{rrj} for each root p_j (in the cases of $k_{12} < 1$ and $k_{12} > 1$ under existing interface at $\gamma = -(\varphi_1 + \varphi_2)/3$)

Root	Distribution of stress intensity K_{rrj}	
	$k_{12} < 1$ $(G_1 < G_2)$	$k_{12} > 1$ $(G_1 > G_2)$
p_1	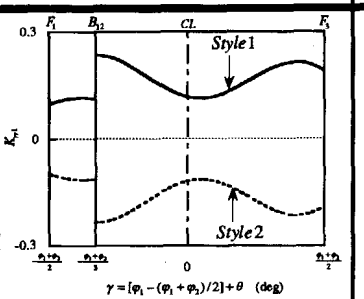	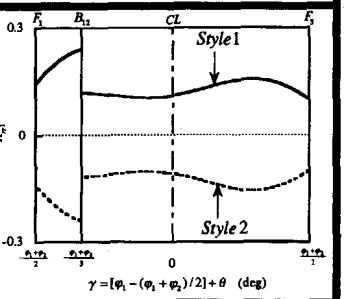
p_2	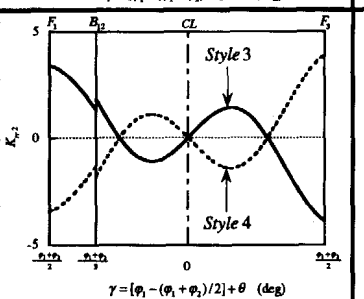	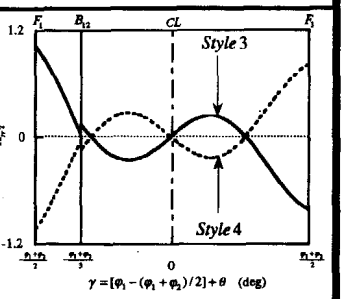
p_3	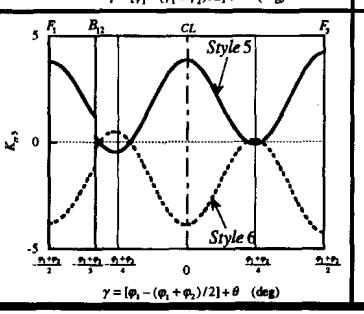	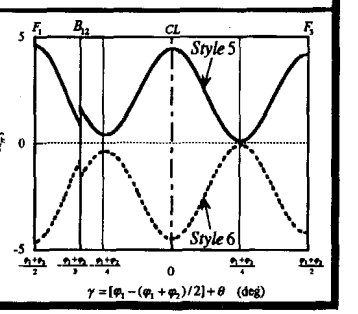

Table A3. Distribution forms of the stress intensity $K_{r\theta j}$ for each root p_j

Root	Distribution of stress intensity $K_{r\theta j}$
p_1	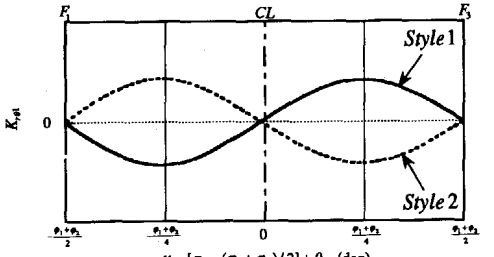
p_2	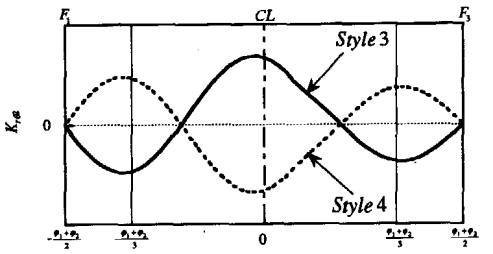
p_3	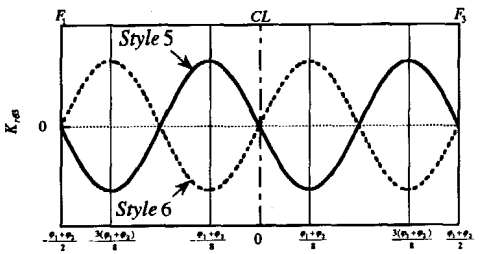

Table A4. Distribution forms of the stress intensity $K_{\theta\theta j}$ for each root p_j

Root	Distribution of stress intensity $K_{\theta\theta j}$
p_1	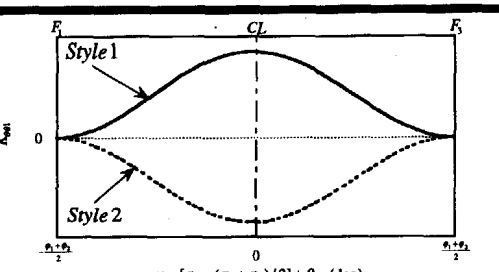
p_2	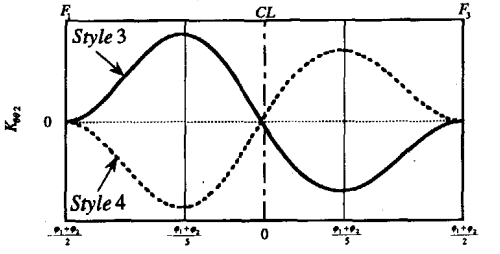
p_3